Anal. Chem. **2007,** *79,* 5529−5539

Accelerated Articles

Protocols for Three-Dimensional Molecular Imaging Using Mass Spectrometry

Andreas Wucher,[†] Juan Cheng,[‡,§] and Nicholas Winograd*[,‡]

Department of Chemistry, Penn State University, 104 Chemistry Building, University Park, Pennsylvania 16802, and Physics Department, University of Duisburg-Essen, 47048 Duisburg, Germany

A protocol for three-dimensional molecular thin-film analysis is described that utilizes imaging time-of-flight secondary ion mass spectrometry and large-area atomic force microscopy. As a test study, a 300-nm trehalose film deposited on a Si substrate was structured by bombardment with a focused 15-keV Ga^+ ion beam and analyzed using a 40-keV C_{60}^+ cluster ion beam. A three-dimensional sputter depth profile was acquired as a series of high-resolution lateral SIMS images with intermittent erosion cycles. As the most important result of this study, we find that the structured film exhibits a highly nonuniform erosion rate, thus preventing a simple conversion of primary ion fluence into eroded depth. Instead, the depth scale calibration must be performed individually on each pixel of the imaged area. The resulting laterally resolved depth profiles are discussed in terms of the chemical damage induced by the Ga^+ bombardment along with the physics of the C_{60}^+ induced erosion process.

Erosion of solids with cluster ion beams followed by analysis with secondary ion mass spectrometry (SIMS) is emerging as a powerful strategy for the in-depth characterization of complex organic and inorganic materials.[1−10] In the past with atomic ion bombardment, chemical damage buildup masks chemical information before erosion is even initiated.[11] With cluster ion bombardment, however, it is often observed that the damage is removed at a faster rate than it is created.[12−16] As a consequence, chemical information is preserved during the depth profiling process. The depth information itself is inferred from correlations between the removal rate of the material, the magnitude of the incident ion current, and the time of bombardment. For single-component systems that are not prone to form topological features, this information is relatively straightforward to acquire since cluster bombardment removes material at a spatially uniform rate.[17−19] Using a 300-nm peptide-doped trehalose thin film on Si, for example, a depth resolution of 15−20 nm is observed at the film−Si boundary when eroding with 20-keV C_{60}^+ projectiles.[3,17−19] Similar observations have been made for multilayer polymer films bombarded with (SF_5^+).[8]

A defining characteristic of time-of-flight (TOF)-SIMS experiments is the capability to obtain molecule-specific images by using

* To whom correspondence should be addressed. E-mail: nxw@psu.edu.
† University of Duisburg-Essen.
‡ Penn State University.
§ Current address: Merck & Co., Inc., WP78-210, 770 Sumneytown Pike, West Point, PA 19486.

(1) Gillen, G.; Simons, D. S.; Williams, P. *Anal. Chem.* **1990**, *62*, 2122−30.
(2) Cheng, J.; Wucher, A.; Winograd, N. *J. Phys. Chem. B* **2006**, *110*, 8329−36.
(3) Cheng, J.; Winograd, N. *Anal. Chem.* **2005**, *77*, 3651−9.
(4) Fletcher, J. S.; Lockyer, N. P.; Vaidyanathan, S.; Vickerman, J. C. *Anal. Chem.* **2007**, *79*, 2199−206.
(5) Mahoney, C. M.; Roberson, S. V.; Gillen, G. *Anal. Chem.* **2004**, *76*, 3199−207.
(6) Mahoney, C. M.; Fahey, A. J.; Gillen, G. *Anal. Chem.* **2007**, *79*, 828−36.
(7) Sostarecz, A. G.; McQuaw, C. M.; Wucher, A.; Winograd, N. *Anal. Chem.* **2004**, *76*, 6651−8.
(8) Wagner, M. S. *Anal. Chem.* **2005**, *77*, 911−22.
(9) Wucher, A.; Sun, S. X.; Szakal, C.; Winograd, N. *Anal. Chem.* **2004**, *76*, 7234−42.
(10) Debois, D.; Brunelle, A.; Laprevote, O. *Int. J. Mass Spectrom.* **2007**, *260*, 115−20.
(11) Benninghoven, A. *Surf. Sci.* **1994**, *300*, 246−60.
(12) Wucher, A. *Appl. Surf. Sci.* **2006**, *252*, 6482−9.
(13) Czerwinski, B.; Delcorte, A.; Garrison, B.; Samson, R.; Winograd, N.; Postawa, Z. *Appl. Surf. Sci.* **2006**, *252*, 6419−22.
(14) Smiley, E. J.; Postawa, Z.; Wojciechowski, I. A.; Winograd, N.; Garrison, B. J. *Appl. Surf. Sci.* **2006**, *252*, 6436−9.
(15) Fletcher, J. S.; Lockyer, N. P.; Vickerman, J. C. *Surf. Interface Anal.* **2006**, *38*, 1393−400.
(16) Winograd, N. *Anal. Chem.* **2005**, *77*, 142A−9A.
(17) Sun, S.; Wucher, A.; Szakal, C.; Winograd, N. *Appl. Phys. Lett.* **2004**, *84*, 5177−9.
(18) Seki, T.; Matsuo, J. *Nucl. Instrum. Methods Phys. Res., Sect. B* **2004**, *216*, 191−5.
(19) Aoki, T.; Matsuo, J. *Nucl. Instrum. Methods Phys. Res., Sect. B* **2004**, *216*, 185−90.

10.1021/ac070692a CCC: $37.00
Published on Web 06/21/2007

focused probes to define the location of desorbed molecular ions. With modern cluster ion sources, the probe may be constrained to a diameter of less than 1 μm, providing high lateral definition of the chemistry of the sample surface, with mass spectral information available at every pixel in the resulting image.[20] The combination of imaging SIMS with molecular depth profiling to create three-dimensional information is an obvious and exciting extension of these experiments. Preliminary three-dimensional imaging studies are underway at a number of laboratories.[4,21−23]

Although high erosion rates, low chemical damage accumulation, and reduced topography formation are all properties that favor successful three-dimensional imaging experiments, a number of studies have shown that the sputtering yield of molecular species can vary significantly depending largely upon the mass and matrix of the target molecule.[3,24] For example, the yield of trehalose from pure trehalose films is reduced by nearly a factor of 2 when the film is doped by only 1% peptide.[3,23] The presence of metal overlayers has been shown to quench molecular ion signals to the point where they are unrecoverable,[25] greatly reducing the erosion rate and effectively reducing the molecular ion yield to zero. If these sorts of effects occur within an image plane during erosion of molecular solids, the depth scale will vary from pixel to pixel. Hence, a simple stacking of these arrays will produce a jumbled convolution of depth information.

In this paper, we examine the effects of differential removal rates in a model multicomponent system and provide a protocol for establishing the accurate depth scale required to reconstruct a true three-dimensional image. The model system consists of a peptide-doped trehalose film that has been patterned in three ways using a 15-keV Ga^+ ion beam. Within this system, using C_{60}^+ to acquire the images, different removal rates are found for the unmodified peptide/trehalose film, for a lightly damaged region of the peptide/trehalose film, and for a heavily damaged area of the same system. Depending upon the region of interest, the removal rate of the various species is as high as ~400 molecules/projectile and as low as zero or even achieving negative values, indicating that material may actually be deposited on the surface instead of being removed.

To account for these variations, the sample is analyzed twice using a large-area scanning atomic force microscope (AFM)—before erosion and after the depth profile has been completed. By combining the AFM and mass spectral information, a depth scale is determined at each pixel. New images are constructed so that each plane contains mass spectral information appropriate for a specific sample depth. Using this procedure, the images are stacked to produce a true three-dimensional representation of the multicomponent sample. The results show unequivocally that this type of correction is necessary to yield interpretable information. For example, it is possible to directly utilize the pixel-specific depth profiles to assess the amount and depth distribution of chemical damage induced by the Ga^+ ion writing experiments. We discuss the implications of these experiments for utilizing cluster SIMS in three-dimensional biological imaging studies.

EXPERIMENTAL SECTION

The experiments were performed using a TOF-SIMS described in detail elsewhere.[26] The system is housed in an ultrahigh-vacuum chamber equipped with a fast load-lock for sample entry and removal. The investigated surface is bombarded with primary ions generated from two different sources. First, a focused beam of 15-keV Ga^+ ions is generated by a commercially available liquid metal ion source (Ionoptika IOG 25).[27] The ion current delivered by this source was ~1 nA into a spot size of ~1 μm. The second source delivers a focused beam of mass-selected 40-keV C_{60}^+ cluster ions (Ionoptika C60-40). The available beam current delivered by this source was ~20 pA into a spot size of roughly 1 μm. Both ion beams were directed to the same area of the investigated surface at an angle of incidence of 45° (Ga^+) or 40° (C_{60}^+) with respect to the surface normal. The scanning optics of both ion sources do not correct for non-normal ion incidence such that a rectangular raster field is produced, with the side along the impact plane elongated by roughly a factor of $\sqrt{2}$. Due to the different azimuthal orientation of the two ion guns, the raster areas covered by both ion beams are rotated with respect to each other by 90°. Secondary ion mass spectra are obtained by operating one of the primary ion beams in a pulsed mode with pulse lengths of ~50 ns. Secondary ions removed from the surface due to the ion impact are extracted into a reflectron-type TOF mass spectrometer by means of a pulsed extraction field. This pulse is switched on ~100 ns after the primary ion pulse, ensuring that the sample is at ground potential during the ion bombardment. The TOF spectrometer is operated at a mass resolution of about $m/\Delta m$ = 2500 and equipped with a microchannelplate detector with 15-keV postacceleration.

The model system investigated here was designed by first spin casting a uniform layer of trehalose doped with a 1% concentration of a peptide (GGYR) onto a Si substrate. Details of the deposition process have been described elsewhere and will not be repeated here.[3] The resulting film of ~300-nm thickness was inspected for uniformity both optically and by a wide area AFM from KLA-Tencor (NanoPix 2100). The images were acquired in contact mode with a spring constant of 4 N/m. This sample was then introduced into the vacuum chamber and subjected to a sequence of patterning treatments using the focused Ga^+ ion beam. For the first step, a uniform ion fluence of 1.5×10^{15} Ga^+/cm^2 was applied by rastering the dc beam across an area of 160×200 μm^2 to create a crater with a depth of 30 nm. In the second step, trenches were etched into parts of this crater by scanning the focused dc beam along a predefined line for a certain amount of time. The pattern of the lines written in this way was arranged to form the letters PSU. The value of the ion fluence was sufficient to erode to various depths in the bottom half of the trehalose film. The dimensions of these features were determined by removing

(20) Schwieters, J.; Cramer, H. G.; Heller, T.; Jurgens, U.; Niehuis, E.; Zehnpfenning, J.; Benninghoven, A. *J. Vac. Sci. Technol., A* **1991**, *9*, 2864−71.

(21) Gillen, G.; Fahey, A.; Wagner, M.; Mahoney, C. *Appl. Surf. Sci.* **2006**, *252*, 6537−41.

(22) Kozole, J.; Szakal, C.; Kurczy, M.; Winograd, N. *Appl. Surf. Sci.* **2006**, *252*, 6789−92.

(23) Jones, E. A.; Fletcher, J. S.; Thompson, C. E.; Jackson, D. A.; Lockyer, N. P.; Vickerman, J. C. *Appl. Surf. Sci.* **2006**, *252*, 6844−54.

(24) Hagenhoff, B.; Pfitzer, K.; Tallarek, E.; Kock, R.; Kersting, R. *Appl. Surf. Sci.* **2004**, *231−2*, 196−200.

(25) Cheng, J.; Winograd, N. *Appl. Surf. Sci.* **2006**, *252*, 6498−501.

(26) Braun, R. M.; Blenkinsopp, P.; Mullock, S. J.; Corlett, C.; Willey, K. F.; Vickerman, J. C.; Winograd, N. *Rapid Commun. Mass Spectrom.* **1998**, *12*, 1246.

(27) Weibel, D.; Wong, S.; Lockyer, N.; Blenkinsopp, P.; Hill, R.; Vickerman, J. C. *Anal. Chem.* **2003**, *75*, 1754−64.

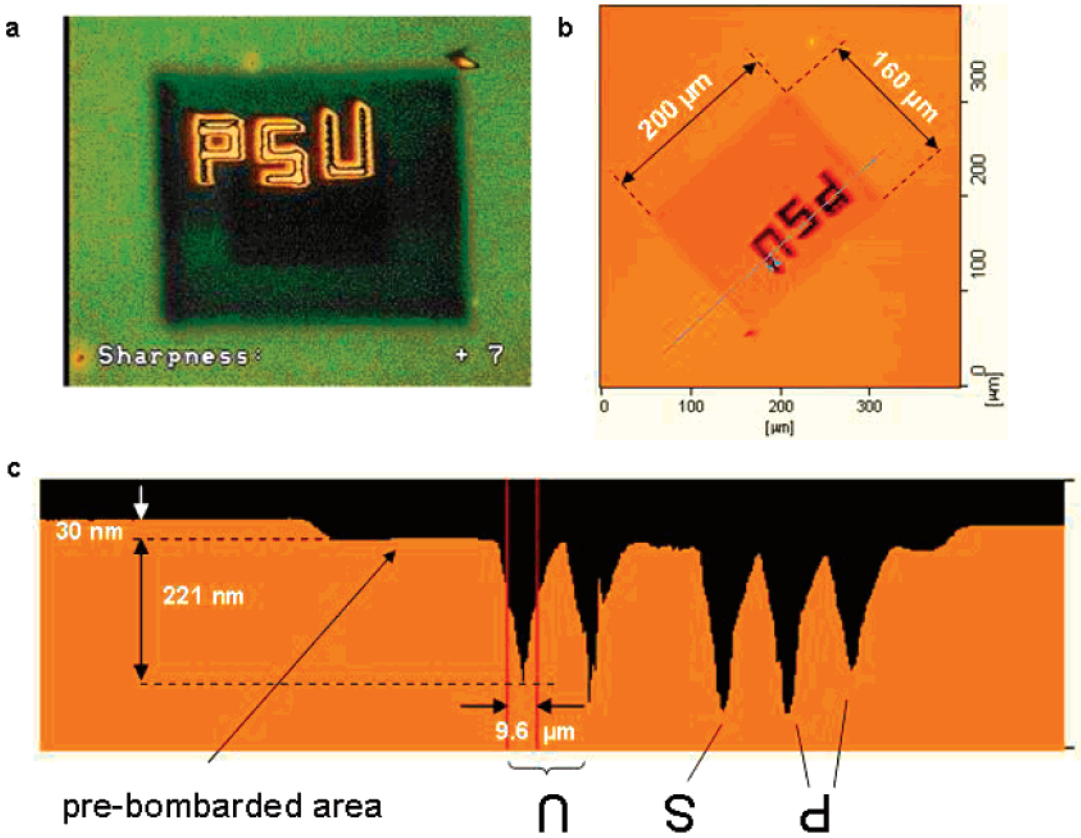

Figure 1. Optical image (a) and AFM image (b) of the patterned trehalose/GGYR layer before depth profiling. (c) provides a line scan along the line indicated in (b). Note that the depth scale is greatly expanded relative to the lateral scale. Since the trenches are really quite wide relative to the AFM tip shape, depth measurements to an accuracy of ~1 nm are possible to achieve in this region.

the sample from the vacuum chamber and analyzing the surface topography by AFM. After the AFM measurements, the sample was reintroduced into the vacuum system and subjected to an imaging sputter depth profile analysis using the 40-keV C_{60}^+ cluster ion beam.

The depth profile was acquired by alternating between sequential data acquisition and sputter erosion cycles. For data acquisition, the C_{60}^+ ion beam was operated in a pulsed mode. A chemical image of the surface was recorded by raster scanning the ion beam in a digital pattern of 256 × 256 pixels over an area of 280 × 200 μm^2, thus matching the pixel size to the dimensions of the ion beam. A total of 20 ion pulses were directed to each pixel. The flight time of each detected ion was recorded using a time-to-digital converter (FAST ComTec GmbH) and stored for later analysis. The total primary ion fluence applied during image acquisition was 1.25 × 10^{10} C_{60}^+/cm^2. Assuming 400 trehalose molecules are removed per C_{60}^+ impact,[2] only 2.6% of a monolayer is removed for each image acquisition and can therefore safely be neglected when computing a depth scale. During the erosion cycles, the C_{60}^+ beam was operated in dc mode and rastered using a TV-like analog pattern with a scan area nearly equivalent to the scan areas utilized during image acquisition. Each erosion cycle comprised a bombardment time of 10 s, corresponding to an ion fluence averaged over the entire raster area of ~2 × 10^{12} C_{60}^+/cm^2 per cycle.

RESULTS AND DISCUSSION

The main focus of this paper is to establish protocols for extracting three-dimensional information from the near-surface region of molecular solids. Since depth information is acquired directly by erosion of the sample by the C_{60} probe, it is obviously essential that the erosion rate be precisely characterized over the entire interrogated area. There is mounting evidence that this rate can be highly nonuniform for multicomponent samples. Hence, the simple process of stacking images as they are acquired during the depth profile may lead to a meaningless convolution of the *x*, *y*, and *z* information.

In this section, a model system is constructed to illustrate the manifestation of nonuniform erosion rates on the resulting three-dimensional output and a strategy is developed for correcting for these effects. The experiment consists of three steps. First, a uniform trehalose layer is patterned using a focused Ga^+ ion beam. The resulting structure is then analyzed by AFM, with results presented in the first subsection. The sample is then reintroduced into the vacuum and subjected to a laterally resolved sputter depth profile using a focused C_{60}^+ ion beam for erosion and analysis. The output from this step is a sequence of high-resolution secondary ion images that are separated by erosion cycles. These sequences, shown in the second subsection, include a three-dimensional graphical representation of the resulting image stack. In a third step, the sample is removed from the vacuum and reanalyzed by AFM in order to determine the surface topography after sputter erosion. Combined with the predepth profiling data, an accurate determination of the eroded sample volume is now possible, leading to a correct depth-scale calibration within each section of the acquired image area. These results are presented in the third subsection.

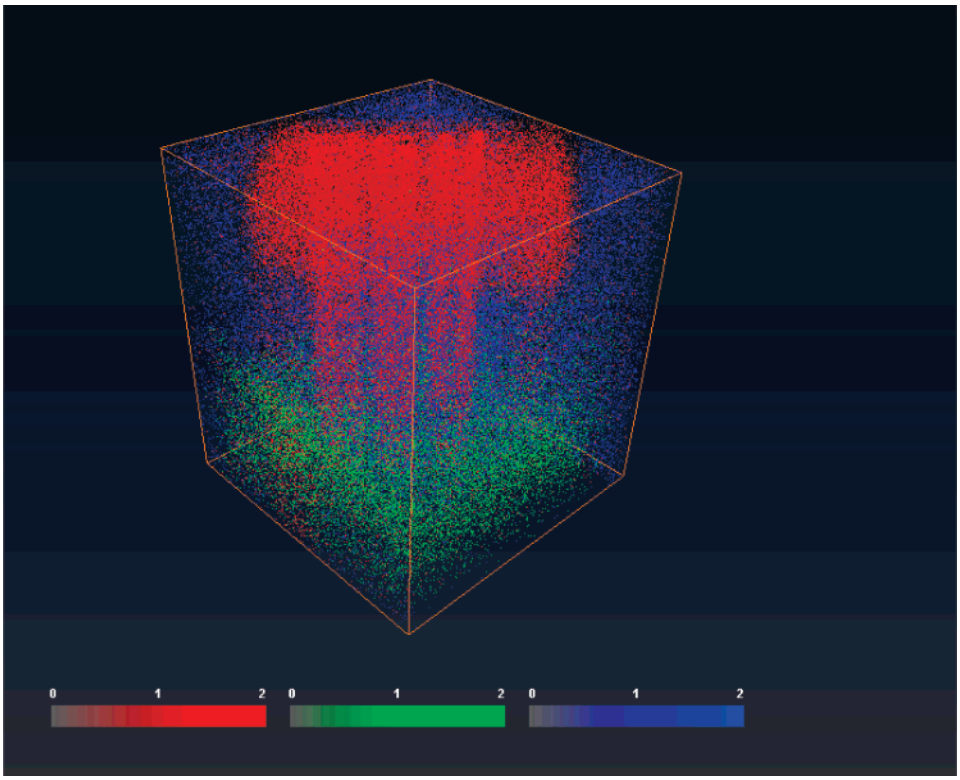

Figure 2. Pseudo-three-dimensional representation of a stack of sequential TOF-SIMS images with equidistant vertical spacing. Red, Ga^+ signal arising from initial Ga bombardment; blue, MH^+ molecular ion signal of GGYR peptide contained in the trehalose overlayer; green, Si^+ signal representing the Si substrate.

1. Film Patterning. A freshly deposited trehalose film doped with 1% GGYR was patterned using a focused beam of 15-keV Ga^+ ions. The pattern was created by bombarding an area of 200 × 160 μm^2 to remove 30 nm of the molecular film. Next, the letters "PSU" were etched into the surface by ion-induced erosion. The letters were created by continuously scanning the Ga^+ ion beam along a series of 12 separate straight lines of width 5 μm and lengths of either 10 or 20 μm. Each line was exposed to the dc ion beam for 5 s.

Images of the resulting structure are displayed in Figure 1. The first panel (a) shows an optical image, which clearly exhibits the interference color changes induced by the varying film thicknesses. Upon careful inspection, it can be seen that the shorter lines are cut deeper into the film than the longer ones. Moreover, the 200 × 160 × 0.03 μm^3 crater created before the letters were written is clearly visible. Also, the trace of a second, smaller raster area is seen within this area. The ion fluence applied to this second area, however, was very small and is neglected in the analysis.

The corresponding AFM image is depicted in panel b. The presence of the 200 × 160 × 0.03 μm^3 crater is clearly visible. From the indicated line scan displayed in panel c, the cross sections of the etched lines are also visible. Note also that the first trench on the right side, corresponding to the 10-μm line in the "P", has a smaller erosion depth than the 5-μm lines in the P. The eroded trenches exhibit a slightly asymmetric triangular lateral profile with half-widths between 6 and 9 μm. The asymmetry is presumably due to the fact that the Ga^+ ion beam is striking the surface at an off-normal angle of incidence, entering from the right-hand side. Hence, sputtered material is ejected in an asymmetric angular distribution. With surface topography developing during the etching process, part of this material may be redeposited on the walls of the evolving trenches, leading to the observed asymmetric etch profile.

The line scan shows that the Ga-bombarded area has been etched to a crater depth of 30 nm. The erosion depth in the center of the trenches varies between 210 and 310 nm as measured from the original surface outside the prebombarded area. This result shows that in the center parts of the 5-μm lines the trehalose overlayer of 300-nm nominal thickness has been completely etched directly to the silicon substrate. Some of the trenches are enclosed well within the trehalose layer. For example, the etched depth of the 10-μm line of the P is 210 nm, ~90 nm from the Si surface.. The lateral dimensions of that line are 40 μm × 9 μm. In connection with the Ga^+ ion current of 1 nA, this converts to an applied ion fluence f of 9×10^{15} Ga^+/cm^2 or an erosion rate dz/df = 2.1 nm^3. Using the molecular density of trehalose (2.7 nm^{-3}), there are six molecular equivalents removed per Ga^+ ion impact.

2. Image Acquisition. A total of 102 secondary ion images were acquired and saved in the course of the depth profile analysis. The images are separated by erosion cycles of 11 s each, thus yielding a total sputter time of 1100 s. The data acquisition was stopped when the SIMS signals characteristic of the overlayer material had disappeared and those representing the substrate had appeared on almost all pixels, indicating the complete removal of the overlayer. Each image was acquired with 256 × 256 pixels and a field of view of 200 μm × 280 μm.

The flight times of all detected ions were stored for each pixel of each image. The body of acquired data can therefore be subsequently analyzed to provide various types of information,

e.g., the mass spectrum at each pixel, lateral images, or vertical depth profiles of selected mass ranges or a combination thereof. For the purpose of this work, we analyze those molecular ions in the mass spectrum that are characteristic of pure trehalose $(M - OH)^+$ at m/z 325), the GGYR peptide (MH^+ at m/z 452), the silicon substrate (Si^+ at m/z 28), and implanted gallium (Ga^+ at m/z 69), respectively. By comparing spectra acquired in different lateral areas and depths, great care was taken to separate these signals from interfering masses of the same nominal m/z.

As a first step in the data analysis, lateral distributions of the selected ion signals were extracted from the data set and combined into an image stack as displayed in Figure 2. In order to visualize the behavior of different layers, the signals representing Ga at m/z 69, peptide at m/z 452, and Si at m/z 28 have been overlaid in red, blue, and green, respectively. It is clearly seen that the Ga^+ secondary ion signal is localized inside the eroded trenches and in the 30-nm surface crater. Interestingly, the molecular ion signals of both the trehalose (m/z 325) and the embedded peptide (m/z 452) are absent in these areas, indicating that the Ga^+ ion bombardment had produced sufficient chemical damage to destroy the molecular integrity of the sample. Outside the Ga-bombarded region, on the other hand, these signals are clearly visible. After a sputter time of 250 s, peptide and trehalose signals appear within the Ga-bombarded area, while the Ga^+ ion signal disappears. Qualitatively, this finding implies that the C_{60}^+ ion erosion removes the layer damaged by the Ga^+ bombardment, exposing the undamaged film underneath. At the end of acquisition, the signals associated with the trehalose overlayer disappear and the Si^+ signal representing the underlying silicon substrate is observed as expected.

3. Depth Scale Calibration. Although the pseudo-three-dimensional representation depicted in Figure 2 provides some qualitative insight, there are more steps required to achieve the desired result. The crucial goal is to evaluate the z coordinate perpendicular to the surface (in the following called "height") at which a particular voxel was acquired. Three factors determine the height of a voxel (i,j,k) corresponding to a particular pixel (j,k) in an acquired image (i). First, the topography of the original surface prior to sputter depth profiling must be known. In the present experiment, we determine this topography from the AFM image shown in Figure 1. Second, the projectile ion fluence applied in the depth profiling experiment must be converted into eroded depth. In general, this depth-scale calibration will be nonlinear, since the erosion rate can vary significantly between different vertical layers. Moreover, erosion rates can in principle also vary between different lateral areas of the sample, thus making the depth progression between subsequently acquired images pixel dependent.

In order to address the depth-scale calibration, regional erosion time profiles are extracted from the data. In the present case, three different lateral regions of the surface are of interest, namely (1) the area where the virgin overlayer is still present, (2) the region where the original surface was subjected to low-dose Ga^+ ion bombardment, and (3) the regions inside the heavily etched trenches. A regional profile is constructed by plotting the intensity of a particular secondary ion signal summed over all pixels of a certain surface area as a function of the erosion time (or ion fluence) at which an image was acquired. For the signals of interest here, such profiles for the two regions 1 and 2 indicated in Figure 3 are shown in Figure 4.

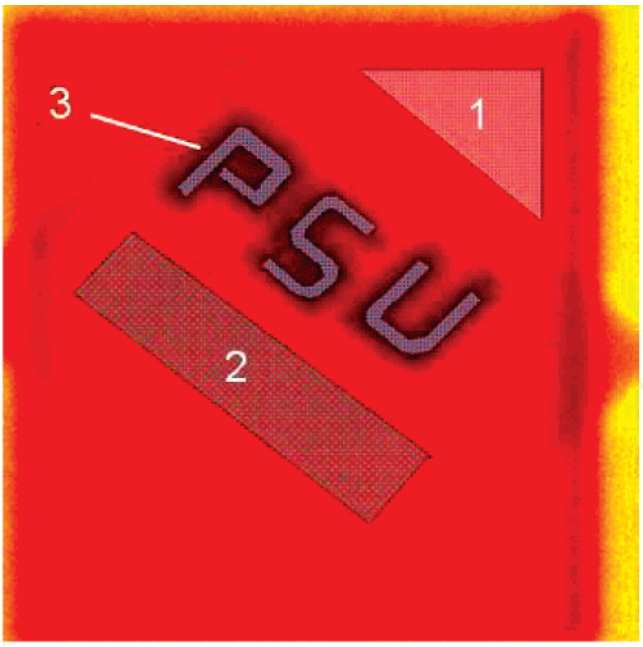

Figure 3. Total ion image, i.e., the signal intensity of all ions (regardless of mass and image number) detected in a specific lateral pixel. The marked regions indicate different areas where regional depth profiles were extracted from the data.

3.1. Region 1. This depth profile exhibits features similar to those measured on unpatterned samples of this kind.[3] The molecular ion signals of trehalose (m/z 325) and the embedded peptide (m/z 452, not shown) track with each other and achieve steady state throughout the removal of the layer, followed by a sharp decrease at the interface to the underlying substrate. At the same time, the Si^+ signal (m/z 28) representing the substrate rises sharply. The depth-scale calibration is relatively straightforward in this lateral region. It must of course be taken into account that the erosion rate varies strongly between the overlayer and the substrate. In line with previous work,[2] we therefore interpolate the erosion rate in the interface region between sputtering times of 650 and 810 s according to

$$\dot{z} = \dot{z}_{\mathrm{Tre}}\left(1 - \frac{I_{\mathrm{Si}^+}}{I_{\mathrm{Si}^+}^{\max}}\right) + \dot{z}_{\mathrm{Si}}\frac{I_{\mathrm{Si}^+}}{I_{\mathrm{Si}^+}^{\max}} \qquad (1)$$

where $I_{\mathrm{Si}^+}^{\max}$ denotes the maximum of the Si^+ ion signal after the interface. For all times up to 650 s, the erosion rate is taken to be constant at the value $\dot{z}_{\mathrm{Tre}}$ corresponding to the pure trehalose/peptide layer, whereas for times after 810 s, a constant value $\dot{z}_{\mathrm{Si}}$ for pure silicon is assumed. The latter, in turn, is estimated from the measured sputter yield Y_{Si} of silicon as

$$\dot{z}_{\mathrm{Si}} = \dot{f} Y_{\mathrm{Si}}/n_{\mathrm{Si}} \qquad (2)$$

where $\dot{f}$ denotes the C_{60}^+ ion flux density and $n_{\mathrm{Si}} = 5 \times 10^{22}$ cm^{-3} is the silicon atom density. Under the prevailing experimental conditions, $Y_{\mathrm{Si}} \sim 200$ atoms/ion and $\dot{f} = 2.5 \times 10^{11}$ C_{60}^+/cm^{2}s, yielding $\dot{z}_{\mathrm{Si}} \approx 0.01$ nm/s. Therefore, only ~3.4 nm of silicon is

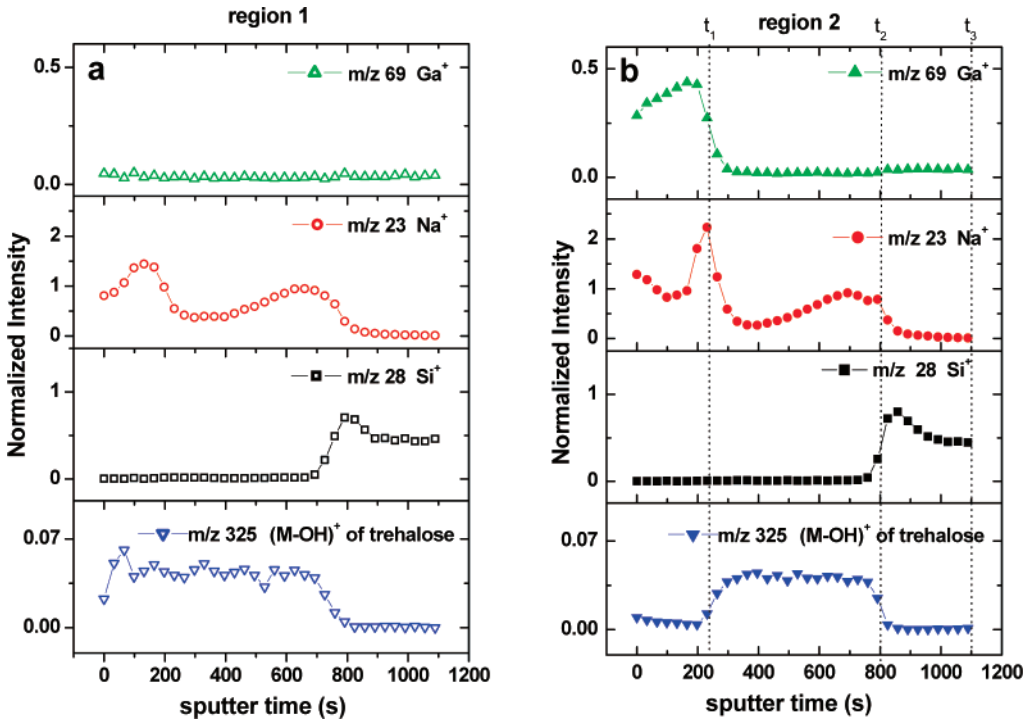

Figure 4. Regional sputter time profiles extracted from the acquired image stack. Shown are the signal intensities of different mass peaks summed over all pixels of the lateral regions 1 and 2 (indicated in Figure 3) as a function of sputter time.

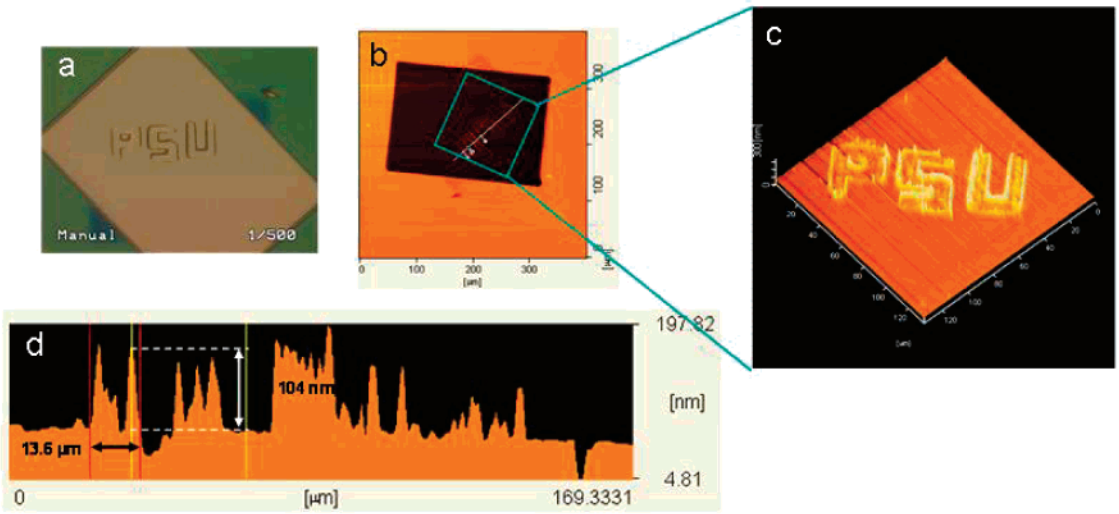

Figure 5. Optical image (a) and AFM topography image (b) of the surface after sputter depth profiling. The marked region of the AFM image is zoomed in and a three-dimensional visualization of the zoomed image is shown in (c). The lower panel provides depth information from (d) as a scan along the line indicated in the AFM image.

removed during the time interval between the interface (at 750 s) and the end of the profile (at 1089 s).

For a quantitative determination of the depth scale, further information about the entire eroded depth is needed. For that purpose, the surface topography was measured again after completion of the depth profile. The respective images are shown in Figure 5. The eroded crater is clearly seen in the optical as well as in the AFM image. From the line scan across the crater depicted in Figure 6, the total crater depth is measured as d = 286 nm. Corrected for the silicon removal, this yields an erosion rate of $\dot{z}_{\mathrm{Tre}} = 0.37$ nm/s or a total sputter yield of ~400 molecule equivalents of trehalose per C_{60}^+ impact for the undisturbed overlayer. With this value, the erosion time axis in Figure 4 can now be converted into a true depth scale.

The resulting depth profiles are shown in Figure 7 (open symbols). Apart from the peptide and substrate signals, the intensity variation of two other secondary ions (Ga^+ and Na^+) is shown. It is seen that the Ga^+ signal is practically negligible in region 1, since this area was never exposed to the gallium ion beam. Second, the Na^+ ion signal exhibits an interesting profile with broad maximums at a depth of ~50 nm and at the interface to the substrate. The exact cause for this behavior is not known

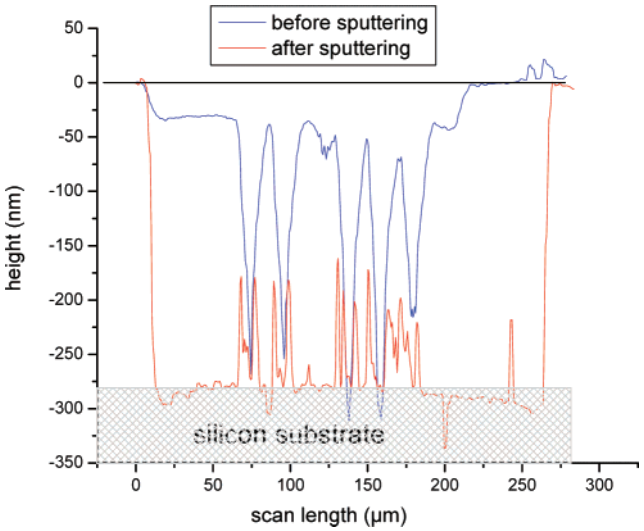

Figure 6. AFM line scans across the analyzed surface area prior to (red) and after sputter depth profiling (black). The scan lines are depicted in Figure 1 and Figure 5, respectively. The data are taken outside the patterned area (a) and across the "PSU" patterned area (b). The dip at 200 nm and the spike at 245 nm are artifacts arising from a scratch and a dust particle, respectively.

at the present time. Nevertheless, we believe this profile to be a characteristic of the undisturbed layer and utilize it as a marker for comparison with region 2.

3.2. Region 2. In this lateral region, the depth-scale calibration is more complicated. At the beginning of the profile shown in Figure 4, erosion proceeds through the Ga-bombarded material, which is apparently heavily doped with Ga. In this regime, the molecular ion signals representing the trehalose/peptide overlayer are very low, indicating severe chemical damage induced by the Ga^+ impact. Both factors lead to an altered erosion rate when compared to the undisturbed film. For sputter times larger than 290 s, on the other hand, the Ga signal disappears and the trehalose/peptide molecular ion signals rise to the same level as in the undisturbed film. Therefore, we conclude that the film is removed with the same erosion rate as in region 1, until the substrate is reached after 800 s. Across the interface, the same interpolation as employed with the data from region 1 is applied using eq 1.

An essential, but so far unknown quantity is the erosion rate within the Ga-doped/damaged layer. The thickness of this altered layer can be determined from the total crater depth (d_{crater}), the original crater depth eroded by the Ga^+ bombardment (d_{Ga}), the total eroded depth in the undisturbed trehalose/peptide layer (d_{Tre}), and the Si removal depth (d_{Si}) as

$$d_{Tre/Ga} = d_{crater} - d_{Ga} - d_{Tre} - d_{Si} \qquad (3)$$

The values of d_{crater} and d_{Ga} are extracted from the measured AFM data reported in Figure 6. The erosion depths d_{Tre} and d_{Si}, on the other hand, can be determined from the known erosion rates

$$d_{Tre} = (t_2 - t_1) \times 0.37 \text{ nm/s}$$

and

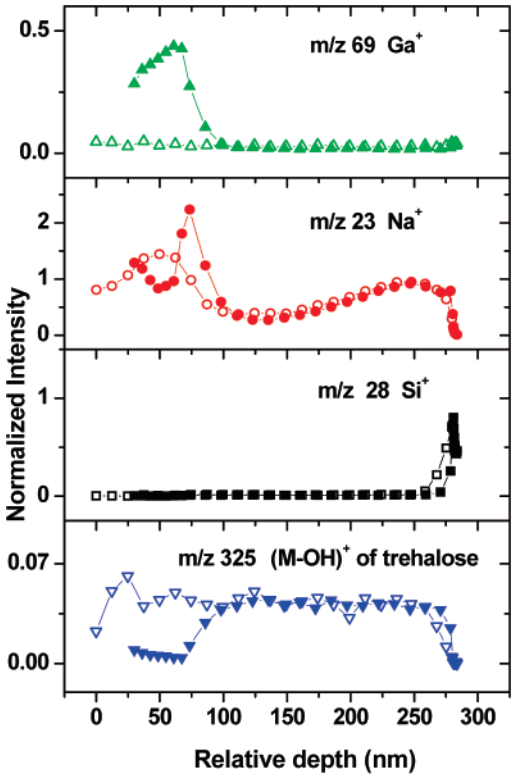

Figure 7. Regional SIMS depth profiles converted from the data presented in Figure 4 after the depth-scale calibration described in the text.

$$d_{Si} = (t_3 - t_2) \times 0.01 \text{ nm/s}$$

where t_1 denotes the time at which the interface between Ga-doped and pure trehalose layer is reached, t_2 marks the interface to the Si substrate, and t_3 is the total sputter time as given in Figure 4. Inserting the respective values, we arrive at an altered layer thickness of $d_{Tre/Ga} = 50$ nm. The resulting erosion rate is given by

$$\dot{z}_{Tre/Ga} = \frac{d_{Tre/Ga}}{t_1} = 0.18 \text{ nm/s} \qquad (4)$$

Hence, the depth scale in region 2 is calibrated as follows. First, the interface time t_1 is defined as the time where the Ga^+ ion signal has fallen to half of its maximum value. For sputter times up to t_1, the erosion rate according to eq 4 was applied. At t_1, the erosion rate is switched to that of the undisturbed trehalose/peptide film, until at the interface to the Si substrate the same interpolation as in region 1 is performed (eq 1). Finally, the Ga-eroded crater depth d_{Ga} is added to all calculated depth values. The resulting depth profiles are shown as closed symbols in Figure 7. Note that no normalization is applied to the trehalose signal except to the number of pixels contained in the two different lateral regions. Moreover, it is interesting to note that the Na^+ ion profile is virtually identical at depths below the layer altered by the Ga^+ ion bombardment. Both observations support our assumption that depth profiling proceeds through an undamaged film in this range. The Ga^+ bombardment does, however, apparently alter the Na depth profile by pushing the Na atoms/ions toward the interface to the undamaged material.

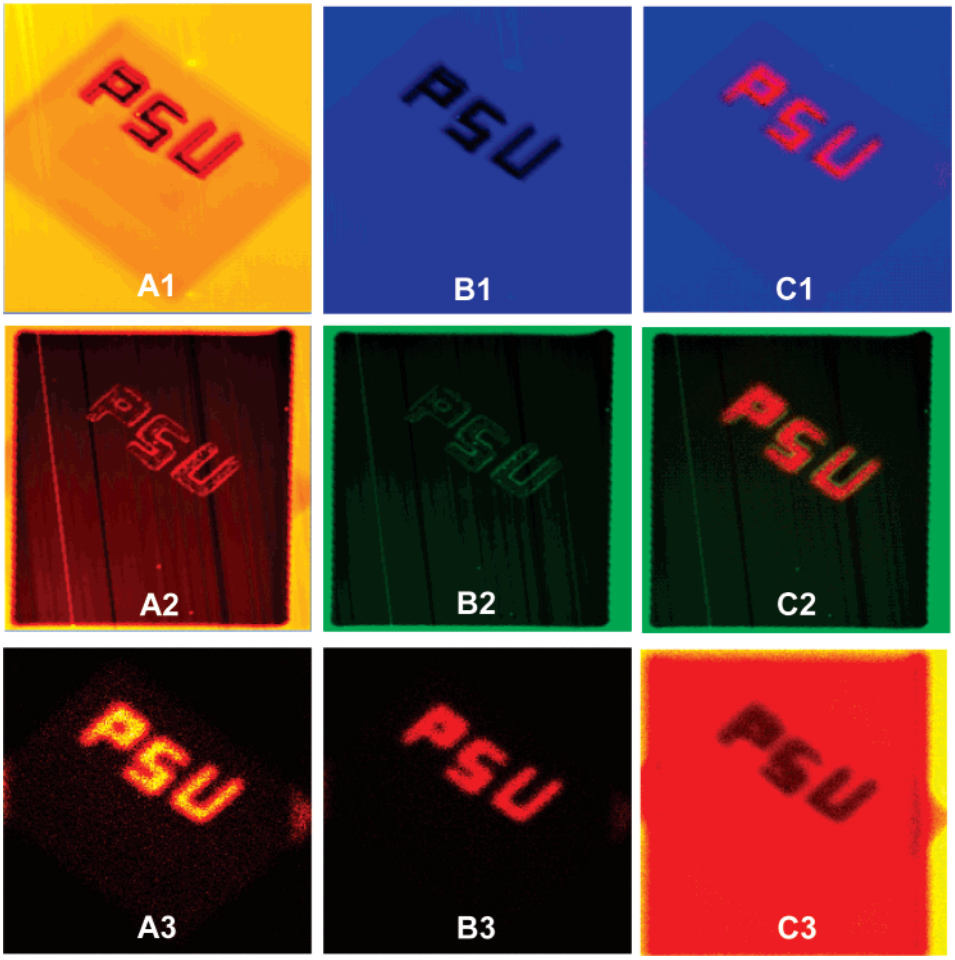

Figure 8. Images to demonstrate zoom and overlay procedure. A1, AFM topography image before depth profiling; A2, AFM topography image after depth profiling; A3, ion image of Ga^+ secondary ions summed over all 102 images; B1 is constructed from A1 after converting the color scale to blue; B2 is constructed from A2 after converting the color scale to green; B3 is constructed from A3 after converting the color scale to red; C1 shows an overlay of B1 and B3; C2 shows an overlay of B2 and B3; C3 shows the total ion image summed over all 102 images in the stack, taken from Figure 3.

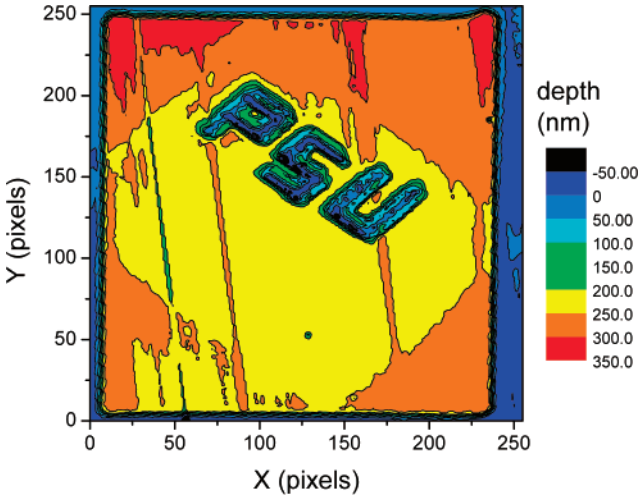

Figure 9. Total eroded depth as a function of lateral position, constructed from the AFM images recorded before and after the molecular depth profile.

The data displayed in Figure 7 reveal unique information about the thickness of the surface layer influenced by the Ga^+ bombardment. To our knowledge, this is the first direct experimental determination of such an altered layer thickness in an organic overlayer caused by metal ion bombardment. The computed value of 50 nm appears large. On the other hand, the mean penetration range of 15-keV Ga atoms calculated by the Monte Carlo code SRIM2003 for a target composition resembling an organic material like trehalose is ~16 nm. We find the maximum of the Ga^+ secondary ion signal at a depth of ~30 nm. The value determined here can also be compared to data that were extracted from a detailed analysis of molecular depth profiles in terms of a simple sputter erosion model.[2] The model reveals the altered layer thickness as a fitting parameter, resulting in values of 27 and 49 nm for 25-keV Au_2^+ and Au_3^+, bombardment of the same trehalose layers as investigated here. These values are in qualitative agreement with the data presented here.

3.3. Region 3. Probably the most interesting region is the area around the deep trenches. Both the optical image and the AFM data clearly show that large residues of the original trehalose/peptide film remain even after complete removal of the film in regions 1 and 2. In fact, the zoomed image in Figure 5 reveals a very interesting topography of these residues, looking like a corral surrounding the original trenches. The scan along the indicated line reveals that the residues are as high as 100 nm above the crater bottom, corresponding to more than 1/3 of the

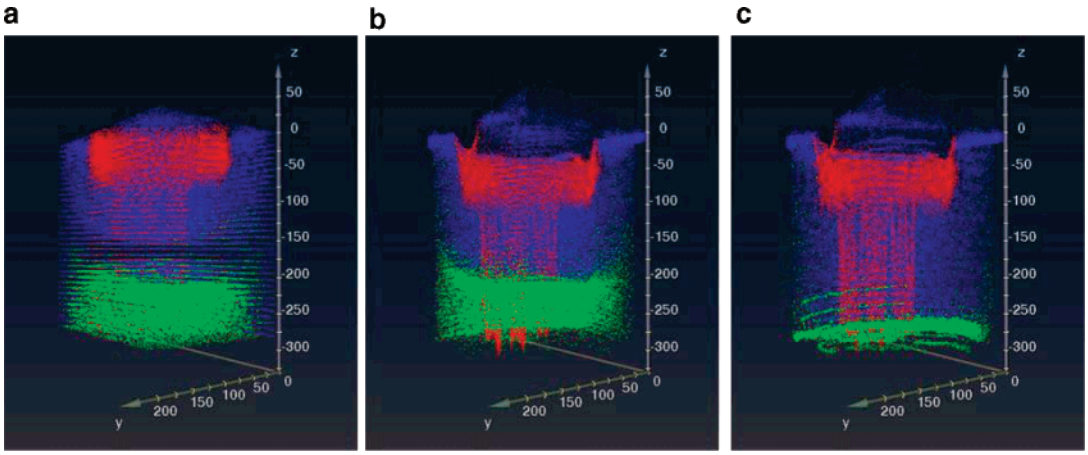

Figure 10. Corrected three-dimensional representation of sample composition as reconstructed from the combined AFM/TOF−SIMS data. The Ga^+ secondary ion signal is depicted in red, the Si^+ substrate ion signal in green, and the MH^+ molecular ion signal of the peptide contained in the trehalose overlayer in blue. Field of view, 200 × 280 μm; total eroded depth, 280 nm. Details of the differences in the representation are given in the text.

original overlayer thickness. From the line scans before and after sputter erosion shown in Figure 6, two points are immediately obvious. First, those trenches that were originally contained within the overlayer have been eroded to the substrate. However, the erosion rate in these heavily bombarded areas is much smaller than in the undisturbed layer. The walls on both sides of the trench profile are not symmetrical, and parts of the wall remain at the same height as they were before the sputter depth profile. In these areas, no net erosion has occurred, even though they were exposed to the same fluence of C_{60}^+ projectile ions as the remainder of the crater. Second, those parts of the deeper trenches that had been previously cut into the silicon substrate appear to be *filled* during the depth profile analysis instead of being eroded. In these regions, the definition of a depth scale obviously loses its sense. As a consequence, depth profiles like the ones depicted in Figure 7 cannot be plotted for region 3.

Although the filling phenomenon resembles the peculiar effects observed by Gillen et al. during sputter depth profiling of silicon with C_{60} projectiles,[28−30] the situation here is observed under considerably different conditions. They found that below a threshold impact energy of ~12 keV there is no net erosion, but rather a deposition of material caused by the incorporation of the projectile atoms into the surface. The same effect has also been predicted theoretically.[31] The profiles in Figure 6, however, clearly show that it is possible to erode silicon under the bombarding conditions of 40 keV with a 40° incident angle. Therefore, the filling effect observed here must be induced by the surface topography. Evidently, a fraction of the material removed from faster eroded sample area around the trenches must be redeposited to fill the holes. Inspection of the secondary ion images taken at the end of the depth profile do not reveal enhanced C^+ and C_n^+ signals inside of the former trenches, as might be expected if the filling was due to pure carbon deposition from the C_{60} projectiles. Instead, the mass spectra taken in these regions resemble those of the trehalose layer.

4. Three-Dimensional Data Analysis. In order to arrive at a true three-dimensional representation of the sample composition, the chemistry and topography must be combined to achieve accurate lateral and depth distributions. To merge this information, the SIMS images taken during the depth profile must be overlaid, pixel for pixel, with the AFM images taken before and after the depth profiling. Since orientation and displacement can be different for all three data sets, mathematical transformations are utilized to ensure pixel coincidence. These transformations involve rotation and cropping of the AFM data and the use of arbitrary marker points to ensure proper overlays.

A measure of success of these manipulations is illustrated by the images presented in Figure 8. In the figure, the AFM images before and after the depth profiling are converted to pure colors. Next, they are overlaid onto the Ga^+ secondary ion signal that was obtained by summing the Ga^+ ion intensity for all the images. As shown in Figure 8 C1 and C2, there is excellent lateral matching of the two types of information. Note that the secondary ion images cover a surface area that is slightly larger than the lateral dimensions of the eroded crater as illustrated in Figure 8 A2 and C3. This mismatch arises from the different scanning mechanisms utilized for depth profiling and imaging as noted in the Experimental Section.

The topography images contain all the information necessary to convert voxel numbers (j,k,i) into x, y, and z coordinates. Finally, AFM images typically provide only a relative change in height. To accurately calibrate the z axis, the respective zero of both AFM images is shifted such that the average height of all pixels located outside the bombarded area is the same. The result of this correction is seen in Figure 6, where the depth scale between the two images is directly comparable. As a consequence, subtraction of both images directly reveals the eroded crater depth of each pixel in the lateral images as seen in Figure 9.

If the erosion rates at each pixel were identical, the image in Figure 9 would consist of only a single color. Clearly, the data show that this basic assumption is incorrect. Depending upon the lateral position inside the crater, the total eroded depth spans a

(28) Gillen, G.; Batteas, J.; Michaels, C. A.; Chi, P.; Small, J.; Windsor, E.; Fahey, A.; Verkouteren, J.; Kim, K. J. *Appl. Surf. Sci.* **2006**, *252*, 6521−5.
(29) Krantzman, K. D.; Kingsbury, D. B.; Garrison, B. J. *Appl. Surf. Sci.* **2006**, *252*, 6463−5.
(30) Wucher, A. *Appl. Surf. Sci.* **2006**, *252*, 6482−9.
(31) Krantzman, K. D.; Kingsbury, D. B.; Garrison, B. J. *Appl. Surf. Sci.* **2006**, *252*, 6463−5.

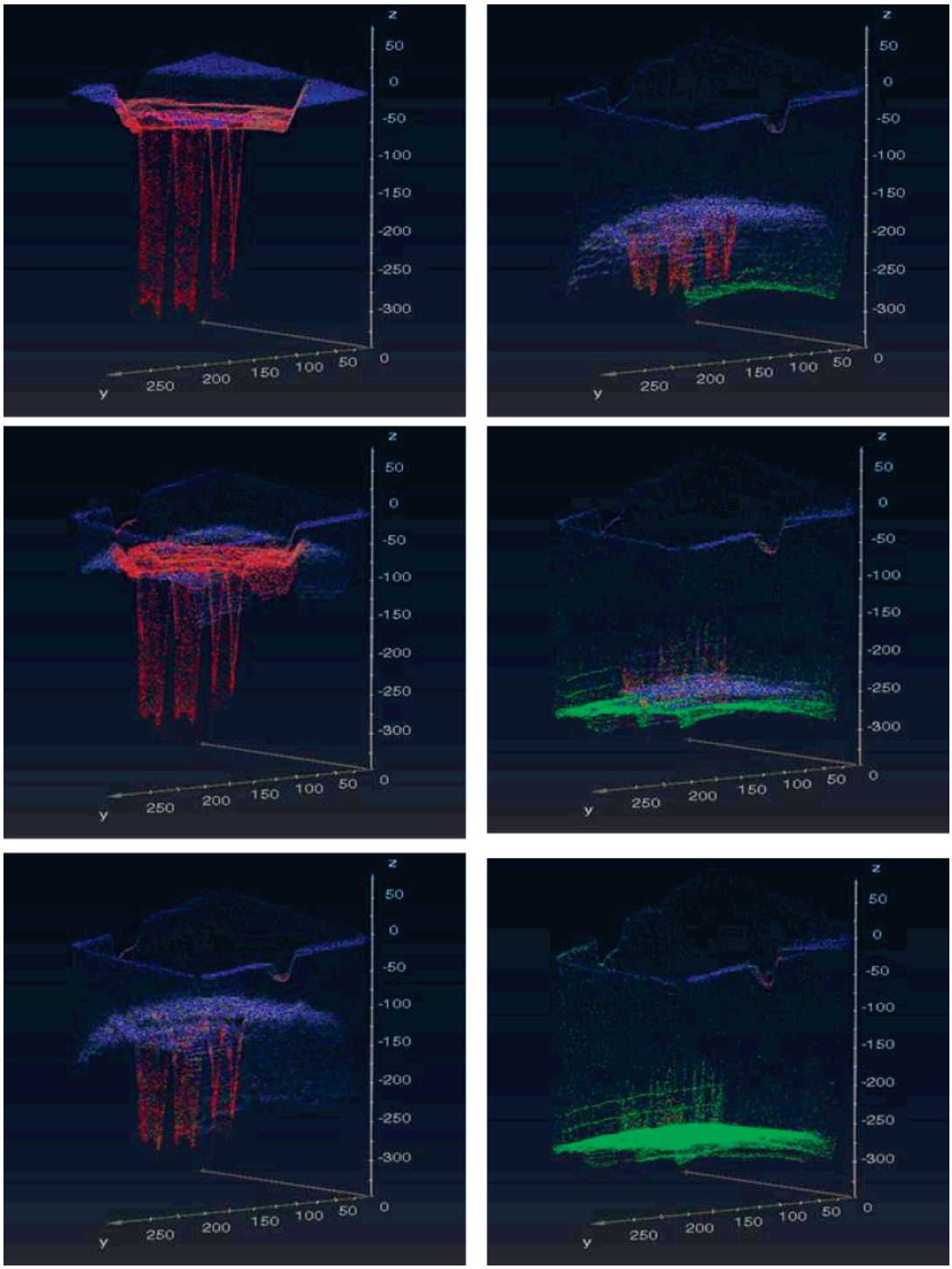

Figure 11. Secondary ion images overlaid with the corresponding surface topography representing different stages of the molecular depth profile analysis. The Ga^+ secondary ion signal is depicted in red, the Si^+ substrate ion signal in green, and the MH^+ molecular ion signal of the peptide contained in the trehalose overlayer in blue. Field of view, 200 × 280 μm; total eroded depth, 280 nm.

range between +300 and −50 nm, where negative values indicate the buildup instead of removal of material during the depth profile. These areas are indicated by the dark blue and black regions. In the remaining part of the crater, erosion depths between zero and 300 nm are observed. This finding is of central importance in converting a pseudo-three-dimensional image to a true three-dimensional representation.

The depth-scale calibration must be performed individually on each lateral pixel of the investigated area. The most direct approach to calculate these erosion rates is to divide the total eroded depth by the total projectile ion fluence at each pixel. Provided the TOF-SIMS images are separated by equal fluence erosion cycles, this results in a constant (but pixel-dependent) height step between subsequent images. The results of this procedure are depicted in Figure 10b, where 34 separate images are included in the data set. It is immediately evident that the three-dimensional representation is much more realistic than the one without inclusion of topography (Figure 10a). In particular,

Ga is seen to be localized in a volume beneath the Ga-eroded shallow crater and in the trenches.

There are still additional artifacts that remain in the data representation depicted in Figure 10b. First, the thickness of the altered layer beneath the Ga^+-bombarded area appears too large when compared to the depth profiles shown in Figure 7. Moreover, close inspection of the Si^+ signal reveals a significant overestimation of the eroded substrate depth. These observations relate to the inherent problem of a depth-dependent erosion rate encountered during depth profile analysis of multilayer samples. In addition, the Si substrate appears to be reached at different depths across the eroded crater. This artifact is due to a lateral inhomogeneity of the primary ion current density across the rastered surface area.[32]

Both effects can be corrected if the nonlinear depth scale calibration described in section 3 is employed on each pixel of the lateral raster area separately. Based on the measured signals of Ga^+, MH^+, and Si^+, the erosion rate should be interpolated between the values appropriate for the undisturbed trehalose layer, the altered layer, and the silicon substrate, respectively, for each pixel of each image. A problem arises due to the small number of secondary ions detected on each pixel, which makes a proper interpolation difficult. Hence, we chose to average the signal over a few neighboring pixels and then simply switch the erosion rate if the average Ga^+ or Si^+ signal exceeded a threshold value of 0.2 counts/pixel. The resulting three-dimensional representation of the data is depicted in Figure 10c. It is seen that the substrate is reached at approximately the correct depth across the entire crater. Moreover, the thickness of the altered layer in the Ga^+ eroded area is consistent with the AFM measurements.

In order to better visualize the data, each secondary ion image is superimposed with the corresponding surface topography and displayed separately. In this way, the entire depth profile can be viewed as a series of sequential images, illustrating the development of the surface topography along with the chemical composition at the momentary surface. While it is impractical to display the entire video, snapshots at particularly interesting points of the profile are shown in Figure 11, using a color scheme identical to that used in Figure 10. It is clearly seen that the first image displays the original surface topography, locating the Ga^+ signal inside the Ga-eroded crater and within the deep trenches, respectively. During the evolution of the profile, it is evident that the virgin trehalose overlayer is more rapidly removed than the Ga^+-altered layer, resulting in a rather flat surface after the altered layer has been removed. While the remaining overlayer is quickly eroded in the regions away from the trenches, no change in height is observed at some points inside the original trenches. At the bottom of the trenches, the surface is seen to move *upward* as depth profiling proceeds.

(32) The cause of this effect is related to the analog TV rastering pattern that was used during the erosion cycles, generating a larger primary ion flux density at the horizontal turning points of the rastered beam. This effect can in principle be avoided if the same digital raster pattern as used for data acquisition is used during the erosion cycles.

CONCLUSIONS

In this work, we have presented a case study of a relatively simple thin-film structure amenable for three-dimensional molecular depth profiling using cluster SIMS. Although the resulting image provides a fairly accurate representation of the composition of this film, the protocols necessary to achieve this meaningful result are certainly not straightforward. Moreover, if the procedures presented here are neglected, as for the pseudo-three-dimensional image of Figure 2, it is easy to be misled about the composition of the sample. For this example, we have chosen materials of widely disparate sputtering properties. For example, the behaviors of Si and the peptide molecular are obviously very different. The addition of Ga atoms to the organic matrix also introduces major complexities. The situation for a purely organic multilayer structure may be somewhat less complicated.

A major motivation for this study is the fact that there is emerging interest in using this technology to provide three-dimensional molecular images of biological cells. In fact, the size of a single cell, and the magnitude of the sputtering fluence of commercially available cluster ion sources, make it feasible to think about eroding through the entire sample, typically to a depth of a few micrometers. Until the differential erosion rate problem noted here can be fully evaluated, however, we suggest that the use of a sensitive topological tool like the AFM is critical for achieving meaningful results. Of particular value is the application of the AFM measurement both before and after the erosion process so that the net erosion rate may be inferred in each pixel of each image in the acquired stack of arrays.

ACKNOWLEDGMENT

The material is based upon work supported by the National Institutes of Health under grant EB002016-13, the National Science Foundation under grant CHE-555314, and the Department of Energy under grant DE-FG02-06ER15803.

Received for review April 9, 2007. Accepted May 29, 2007.

AC070692A